doi: 10.29382/eqs-2018-0126-2

Fault geometrical model of Dujiangyan section in Longmenshan fault zone*

Hu-Rong Duan✉ Sheng-Lei Chen Run Li Quan-Chao Yan

College of Geomatics, *Xi'an University of Science and Technology*, *Xi'an* 710054, *China*

Abstract The focal mechanism solution on the seismic fault plane can reflect the geometric and kinematic characteristics of faults, and it is an important way to further study the fine structure of fault plane. From the focal mechanism solution of the earthquakes around the Dujiangyan fault in Longmenshan fault zone, we derived the average dip angle of Dujiangyan fault is 45.1° based on the seismic moment tensor theory. In order to refine the fault geometry structure, this paper decomposed it into multiple sub-fault planes along the length and width of the fault plane and forms a number of models A13, B13, A23a, A23b, A23c, B23a, B23b and B23c, then calculated the sub-fault's dip of each model. In order to clarify exactly which one of the fault models is closest to the real fault model, the fault slip was carried out for each model in turn, then compared the surface displacement of each model with GPS observations. The results show that B23c model with high dip in shallow and small dip in deep is the best model, the lengths of each sub-fault of Dujiangyan fault from south to north are 33 km, 21 km and 46 km, respectively. When the depth of the fault bottom is about 11 km, the dip angles are 70.56°, 67.41° and 45.55°. When the depth of the fault bottom is about 30 km, The fault dip angles are 44.55°, 29.18° and 44.25°.

Keywords: focal mechanism solution; seismic moment tensor; fault dip; fault fine structure; Dujiangyan fault

1 Introduction

On May 12, 2008, the M_W 7.9 earthquake occurred in the Longmenshan fault zone in China. The earthquake was considered to be the most destructive earthquake event in China in the past 50 years. It caused more than 80,000 people deaths and about 37,000 people were homeless (Xu et al. 2008). The Longmenshan fault zone is on the eastern boundary of the Qinghai-Tibet Plateau and is mainly composed of three major faults. From the east to the west, they are the Longmenshan piedmont fault ($F1$), the Longmenshan main central fault ($F2$), and the Longmenshan Houshan fault ($F3$) Figure 1; Xu et al., 2005. The southern segment and the middle segment (102°E~104.5°E) of the Longmenshan fault are dominated by thrust. The largest earthquake occurred in this region in history was the Wenchuan M_S6.5 earthquake in 1657. The epicentral location of Wenchuan M_W7.9 earthquake is located in the main central fault of Longmenshan, and it is the first thrust-type earthquake that occurred on the inner low-velocity slip fault in the world. Zhang (2008) thought that the seismogenic fault is a shovel structure. The interaction between deep low dip angles and shallow high dip angles controls the breed and occurrence of strong earthquakes. Considering that the seismicity of the Longmenshan fault zone is related to the deformation and support of the Sichuan Plateau and the Sichuan Basin (Zhang et al., 2009), the high and low dip angle reverse fault slips correspond to different mechanical conditions, respectively. The study on the geometry of the seismogenic fault plane are of great significance for understanding the interrelationship between seismogenic units. The scholars have conducted extensive research on the geometry and sliding distribution of the Longmenshan earthquake fault based on spatial geodetic observation data and seismic data, such as Ji and Hayes (2009), which determined the strike of the fault is 229° and dip angle is 33° by waveform inversion, the southern segment is dominated by slip, with a maximum displacement of 9 meters, this viewpoint is consistent with geological result (Burchfiel et al., 2008). Wang et al. (2008) used a far-field wave waveform recording combination with near-field coseismic displacement data, geological data, and surface rupture trajectories formed by earthquakes to construct a double "shovel-like" finite-seismic fault model, determining the strike of 229° and the dip angle of 32°, followed by inversion of fault slip distribution, indicating that the

* **Received** 9 April 2018; **accepted in revised form** 2 August 2018; **published** 5 September 2018.

✉ **Corresponding author. e-mail**: duanhurong@126.com

© The Seismological Society of China and Institute of Geophysics, China Earthquake Administration 2018

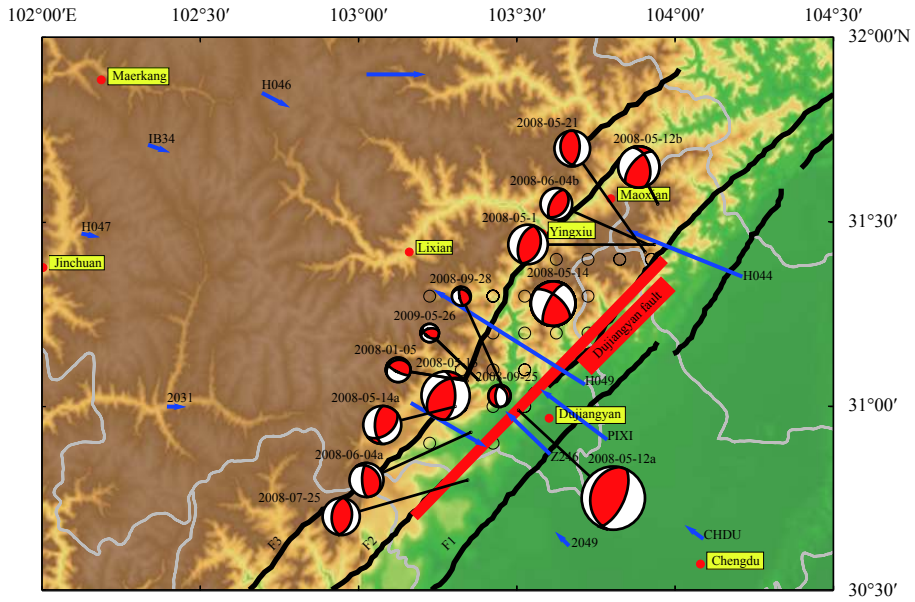


Figure 1 Tectonic setting and fracture distribution of the research area. The black line is the geological fault surface track; the red line is the simplified fault model of the Dujiangyan section of the Longmenshan fault zone; the red source ball is from Table 1, the blue arrow is the GPS observation, and the direction is the azimuth, and the length is the size; the gray circles are positioning results for small earthquakes, the red dots are the location of the cities

southern segment is dominated by slipping. Diao et al. (2010) thought that the width of the fault plane is 40 km, and the dip angle varies linearly with depth from 65° at the ground surface to 20° at the bottom of the fault. The southern section is dominated by slip, and its maximum displacement reaches 5 m. Shen et al. (2009) believed that the dip angle of the main central fault in the Longmenshan Mountains varies along the length of the fault, and the dip angle of the fault in the northern section is close to 90°. The dip angle of the fault in the southern section is relatively small, the southern section of the fault is dominated by slip and the maximum displacement on fault plane is 7 m. The result of Wang et al. (2011) is that the Qingchuan section has a dip angle of 70°, the Yingxiu-Beichuan section has a dip angle of 55°, the Beichuan section has a fault plane width of 70–80 km, and the creep area at the bottom of this section has dip angle of 7° with slipping, the maximum displacement on fault plane is 16 m. The Wenchuan earthquake fracture drilling WFSD-1 and 2 were in the Bajiaomiao village, Hongkou town, Dujiangyan City. The measured results show that the fault tends to the southwest with dip angle of 62° at a depth of about 590 m (Li et al., 2013). Hu et al. (2008) believed that the dip of the source is 30° at a depth of 18 km using the focal mechanism solution given by the first wave of P-waves. The above scholars agree to that the Longmenshan fault geometry has a trend of 229°, a southwest tendency, a fault width of 40 km, and the southern section is mainly by slip. However, there are certain differences between the results in fault dip and maximum slippage. This difference is due to the fact that the sliding distribution obtained from inversion of surface deformation information depends on the differently given geometric model of the fault (Xue et al., 2009a; Li et al., 2011; Tong et al., 2014), although the given sliding distributions can better fit the surface observation data, but its set fault dip angle may have some differences from the actual, resulting in the inversion of the sliding inconsistent with the actual.

One of the great discoveries of seismologists in the 21st century is that most earthquakes occurred on the fault plane and its vicinity. With the improvement of seismic location accuracy, the development of fault plane geometric parameters based on the clustering of small earthquakes was promoted. Hayes and Wald (2010) proposed the maximum likelihood estimation of the subduction zone contact surface based on seismic parameters and the assumption that the earthquake occurred on and near the fault plane. Based on the source distribution data of earthquakes, the maximum likelihood estimation method and its improvement method are successfully applied to the determination of the fault plane dip angle (Wang et al., 2013; Zhang et al., 2013; Sheng, 2015; Gao et al., 2016). Since the average value of the fault plane dip angle is obtained from the seismic cluster data, the fault geometry description is not precise enough. Fortunately, Aki (1966) proposed the theory that the moment tensor of the earthquake is directly related to the physical essence of the fracture rupture process. This theory can accurately infer

the geometric parameters and motion properties of the fault plane (Okal, 1980). The purely biased seismic moment tensor defined by Silver and Jordon (1982) is consistent with the so-called double-strand size. The best double-coupled source is the average shear dislocation, the general dislocation source and the matrix eigenvalue of the seismic moment tensor. The matrix eigenvectors correspond to the relative sizes and directions of the three principal axes *T*, *B*, and *P* of the focal mechanism solution. Frepoli et al. (2017) used the recorded data from the seismic stations of the Yaping-Ning fault zone to calculate multiple focal mechanisms and inferred the geometry of the active faults involved. Based on the multiple focal mechanism solutions near the fault surface of the Dujiangyan segment, this paper refines the fault dip and solves its dip distribution, and inverts the slip of each subfault on the basis of dislocation theory. It is verified by the forward surface displacement that the fault model with dip angle distribution can be better explain surface displacement observations than plane fault model with a single inclination.

2 Data

The seismic positioning data used in this paper was the aftershock data of 4 days after the Wenchuan earthquake with magnitude not lower than 4.0. This data was published by the China Seismological Networks Center. A total of 43 small earthquake sources were selected for the studied area (30.68°N–31.40°N, 103.17°E–103.94°E) (Wang et al., 2010). The coseismic displacement data used in this paper comes from the "China Crustal Movement Observation Network" project of the national major scientific project (China Crustal Movement Observation Network project team, 2008). The GPS observation data was from the national major scientific projects, the national key basic research and development plan projects, China Earthquake Administration, and the Seismological Bureau of Sichuan Province. The data was reliable and have high accuracy. The data processing sampling interval is 30 s, each time period is 24 h, and the double-difference mode is used. The crustal motion velocity field of the region relative to the Eurasian plate was obtained by the GAMIT/GLOBK software. Relative to the long-term deformation velocity field under the ITRF reference framework (Zhang, 2008), the results are shown in Figure 1. In this paper, we studied the 14 focal mechanism solutions for the thrust type from January 2008 to May 2009 around the Dujiangyan section of the fault (Hu et al., 2008; Guo et al., 2010; Cui et al., 2011; Feng et al., 2013). Table 1 shows that the P-wave initial data used in the calculation of the focal mechanism solution are all fine-positioned data and the results are reliable.

3 Theoretical model for determining fault dip angle based on focal mechanism

Assuming that the direction of the tectonic stress field in the study area remains constant during the study period, and the direction of the sliding of the historical earthquake fault is consistent with the shear stress on the fault plane, so the sliding angle of the historical earthquake can be derived (Li et al., 2007). Suppose the tectonic stress field *P* axis azimuth φ_P, angle of depression δ_P, *T* axis azimuth φ_T, and angle of depression δ_T, then the mathematical expression of the direction vector in the northeast geographic coordinate system are

$$\boldsymbol{T} = (\cos\varphi_T \cos\delta_T, \sin\varphi_T \cos\delta_T, \sin\delta_T), \tag{1}$$

$$\boldsymbol{P} = (\cos\varphi_P \cos\delta_P, \sin\varphi_P \cos\delta_P, \sin\delta_P). \tag{2}$$

The direction vector of the intermediate axis (*B*-axis) is expressed as:

$$\boldsymbol{B} = \boldsymbol{P} \times \boldsymbol{T} \tag{3}$$

In a isotropic medium, the sliding of a finite-size plane fault is mechanically strictly equivalent to the double-strand couple distributed on the fault plane. The three characteristics vectors of the seismic moment tensor *M* of a double-coupled source (a shear dislocation source) respectively correspond to the focal and triaxial directions *T*, *B*, *P* of the focal mechanism solution (Silver and Jordon, 1982). Assuming that the scalar seismic momenting M_0 is 1, and the characteristic value of the moment tensor is (1, 0, –1), the seismic moment tensor *M* can be determined according to the characteristic value of the moment tensor. Due to fault displacement of natural earthquakes, stress discontinuities along the normal direction of the fault do not generally exist under large confining pressures, and only pure shear displacement occurs. The relationship between seismic moment tensor *M* and fault dip δ and slip angle λ is expressed as the equation (4), the first two items are strike-slip faults and the last two are dip-slip fault faults.

$$\begin{aligned} M = {} & \cos\delta\cos\lambda M^1 + \sin\delta\cos\lambda M^2 + \\ & \cos 2\delta \sin\lambda M^3 + \sin 2\delta \sin\lambda M^4, \end{aligned} \tag{4}$$

$$\boldsymbol{M}^1 = M_0 \begin{bmatrix} 0 & 0 & -\cos\phi_s \\ 0 & 0 & -\sin\phi_s \\ -\cos\phi_s & -\sin\phi_s & 0 \end{bmatrix},$$

$$\boldsymbol{M}^3 = M_0 \begin{bmatrix} 0 & 0 & -\sin\phi_s \\ 0 & 0 & -\cos\phi_s \\ -\sin\phi_s & -\cos\phi_s & 0 \end{bmatrix}. \tag{5}$$

Table 1 Focal mechanism solutions of Wenchuan earthquake and some of its aftershocks

No.	Shock time a-mo-d	Longitude/°	Latitude/°	Depth (km)	magnitude M_W	Nodal plane A/°			Nodal plane B/°			*P* axis/°		*T* axis/°		*B* axis/°		Label
						Strike	Dip	Rake	Strike	Dip	Rake	Strike	Dip	Strike	Dip	Strike	Dip	
1	2008-06-04	103.33	30.93	11.1	4.3	179	69	106	320	26	54	256	23	114	62	353	15	*
2	2008-05-13	103.18	31.03	13.6	6.1	228	44	129	359	58	58	111	7	216	63	18	26	*
3	2008-05-14	103.28	31.00	14.6	4.8	181	58	57	51	44	131	293	8	38	61	199	27	*
4	2008-05-14	103.91	31.44	15.5	5.0	198	52	90	17	38	89	288	7	110	83	18	0	*
5	2008-07-25	103.32	30.80	15.7	4.7	184	48	86	10	42	94	277	3	53	86	187	3	*
6	2008-06-04	103.89	31.44	15.9	4.0	206	57	84	36	33	99	300	12	97	77	209	5	*
7	2008-05-21	103.88	31.42	17.0	4.5	168	35	76	5	56	100	88	11	306	77	180	8	*
8	2008-05-12	103.48	30.99	12.9	8.0	190	28	77	24	62	97	109	17	310	72	201	6	*
9	2008-09-25	103.42	31.03	11.0	2.8	182	60	-75	335	33	-113	261	13	354	13	126	71	#
10	2008-09-28	103.432	31.05	10.0	2.4	293	29	37	170	73	114	111	55	343	23	242	25	#
11	2008-01-05	103.317	31.07	12.0	3.1	249	21	44	117	76	106	47	57	293	15	194	29	#
12	2009-05-26	103.353	31.07	14.0	2.3	256	49	53	125	53	124	96	63	283	27	191	3	#
13	2008-05-12	103.92	31.55	12.0	5.2	221	61	128	342	46	42	285	8	182	56	20	33	+
14	2008-05-14	103.59	31.28	12.0	5.6	208	69	149	310	61	25	261	5	167	37	357	53	-

Note: The result marked by "*" is from Cui (2011), marked by "#" is from Feng (2013), marked by "+" is from Hu (2008), and marked by "-" is from Guo (2010) solution.

$$\boldsymbol{M}^2 = M_0\begin{bmatrix} -\sin 2\phi_s & \cos 2\phi_s & 0 \\ \cos 2\phi_s & \sin 2\phi_s & 0 \\ 0 & 0 & 0 \end{bmatrix},$$

$$\boldsymbol{M}^4 = M_0\begin{bmatrix} -\sin^2\phi_s & \frac{1}{2}\cos 2\phi_s & 0 \\ \frac{1}{2}\cos 2\phi_s & -\cos^2\phi_s & 0 \\ 0 & 0 & 0 \end{bmatrix}. \quad (6)$$

For a certain strike direction, the seismic moment tensor M is decomposed into two directions of 0° and 45°.

$$\boldsymbol{M} = \boldsymbol{M}^D = \alpha\boldsymbol{M}_0^D + \beta\boldsymbol{M}_{45}^D, \quad (7)$$

$$\boldsymbol{M}_0^D(\delta = 0°) = \begin{bmatrix} 0 & 0 & -\sin\phi \\ 0 & 0 & \cos\phi \\ -\sin\phi & \cos\phi & 0 \end{bmatrix},$$
$$\boldsymbol{M}_{45}^D(\delta = 45°) = \begin{bmatrix} -\sin^2\phi & \frac{1}{2}\sin 2\phi & 0 \\ \frac{1}{2}\sin 2\phi & -\cos^2\phi & 0 \\ 0 & 0 & 1 \end{bmatrix}. \quad (8)$$

According to the linear coefficient the inclination can be determined

$$\delta = \frac{1}{2}\arctan\left(\frac{\beta}{\alpha}\right). \quad (9)$$

When calculating the data of multiple focal mechanism solutions on the fault plane, the dip angle is a weighted average, where ω_i is the weight of the seismic event. In this paper, the value is the square of the earthquake magnitude. The n in the formula is the number of focal mechanism solutions.

$$\hat{\delta} = \sum_{i=1}^{n}\frac{\delta_i\omega_i}{\omega_i}. \quad (10)$$

4 Dujiangyan section fault dip of Longmenshan fault

The fault in the Dujiangyan section of the Longmenshan fault zone is located at the south of the Wenchuan earthquake fault. The starting point of the fault is identified as (103.17°E 30.68°N), and strike is 229°, inclination is southwest , with a length of 100 km and a width of 40 km. The nature of the fault movement is a thrust type and a small amount of strike slip, satisfying the condition of equation (4). The distribution of the focal mechanism solution data across the entire fault plane is shown in Figure 2. The entire fault plane is divided into subfaults according to the models of 1 (row) × 1 (column), 1 (row) × 3 (column), and 2 (row) × 3 (column), and the dip angle of fault plane is solved based on the mechanism contained in each subfaults.

In this paper, the entire fault plane was divided into model A11 according to 1 (row) × 1 (column) (the schematic diagram of the fault plane is shown in Figure 3). The parameters are shown in Table 2. The plane fault dip angle that calculated from equations (1)–(7) is 45.1°. In order to verify the correctness of fault dip results, we used 10 GPS observations such as points H050, H049, PIXI, Z246, etc. We used the Repulsive Particle Swarm (RPS) algorithm combined with finite rectangular dislocation model to invert the slip of the fault (Okada, 1985; Mishra, 2006), because of the shear fracture of the fault, the crushing or tensile components of the fault are not considered. The inversion results are shown in columns 6 and 7 of Table 2, and the forward surface displacements (see black arrows in Figure 5) are based on the inversion results. The near-field point H050 (blue arrows) by model calculations has a good fit to GPS observations. Compared with GPS observations, the calculated values of the model are not only smaller in size but also different in direction at the point Z246 and the point PIXI. However, there is a significant difference

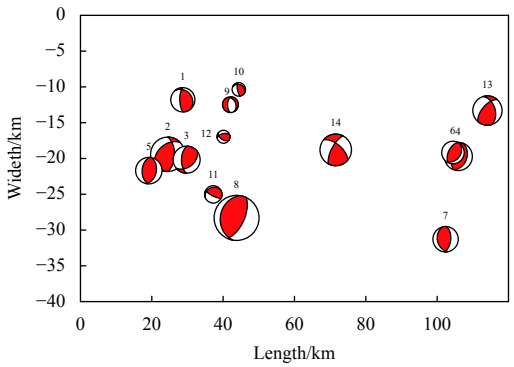


Figure 2 Distribution of focal mechanism on fault plane. The horizontal axis shows the strike direction of the fault, and the length from the fault starting point (southern end) to the end point (north end) is 100 km; the vertical axis is the fault width direction, and the width from the surface to the bottom of the fault is 40 km, and all the focal mechanisms are projected onto this plane. The size of the focal mechanism ball is magnitude, and the number of words on it is the focal mechanism number. The corresponding data is shown in Table 2

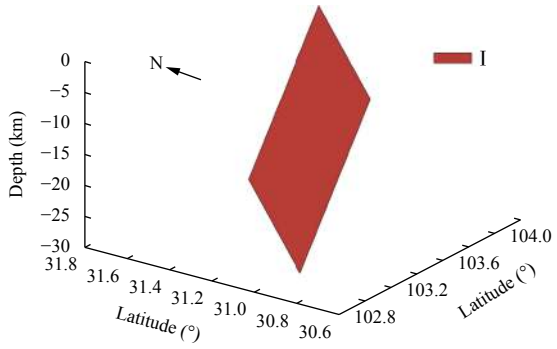


Figure 3 Sub-fault plane of 1 (row) × 1 (column) model schematic

Table 2 Fault geometric model of 1 (row) ×1 (column)

Model	Length (km)	Width (km)	Dip/°	Depth (km)	Strike-slip U_1 (m)	Dip-slip U_2 (m)	Include focal point number	Subfault block number
A11	100.00	40.00	45.10	0.00	–0.20	–2.39	1, 2, 3, 4, 5, 6, 7, 8, 9, 10, 11, 12, 13, 14	I

Note: The depth is the distance from the top of the fault plane to the ground, the strike-slip component is U_1, '+' is left-handed, '–' is right-handed, the d-slip component is U_2, '+' is subduction, '–' is the thrust; the included focal mechanism The point number is shown in the first column of Table 1 (the same below).

between the calculated value of the point H049 and the GPS observation value. Although the directions are basically the same, The size is obviously different, indicating that the fault movement has inhomogeneity and needs to subdivide the fault along the length of the fault plane.

We divided the fault into three sub-faults along the length of the fault plane. When the sub-fault lengths are equal, it is A13 model. When the sub-fault lengths are not equal, it is the B13 model (distribution of each model subfault segment is shown in Figure 4). The specific parameters are shown in Table 3, and the inversion results in the sliding quantity is show in the columns 6 and 7 of Table 3, forward displacement of the surface based on inversion results are shown in Figure 5 (red, green arrows). We found that when using the A13 model, in addition to the significant improvement in the results of the point H049 versus the A11 model, the model calculations for the remaining points such as Z246, PIXI, 2049, and CHDU appear to be worse; when using the B13 model, not only the points H050, Z246, PIXI, 2046, and CHDU are close to the results of the model A11, but also the calculated value of the point H049 is closer to the GPS observation than the A11 model, it is proved that the division of the B13 model in the length direction is more reasonable than that of the A13 model.

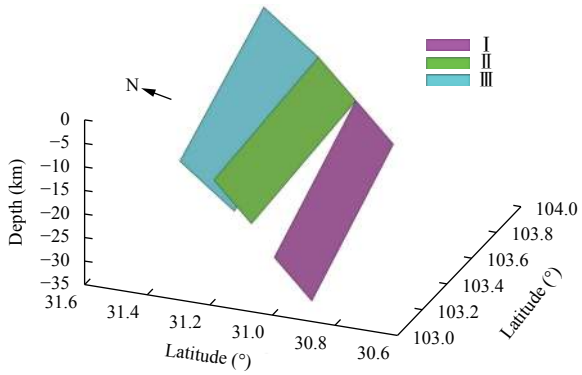


Figure 4 Sub-fault plane of 1 (row) × 3 (column) model schematic

Table 3 Fault geometric model of 1 (row) * 3 (column)

Model	Length (km)	Width (km)	Dip/°	Depth (km)	Strike-slip U_1 (m)	Dip-slip U_2 (m)	Include focal point number	Subfault block number
A13	33.3	40.00	50.14	0.00	–0.35	–3.29	1, 2, 3, 5	I
	33.3	40.00	34.80	0.00	–0.12	–1.23	8, 9, 10, 11, 12	II
	33.3	40.00	48.75	0.00	–1.99	–8.93	4, 6, 7, 13, 14	III
B13	33.0	40.00	50.14	0.00	–0.44	–3.15	1, 2, 3, 5	I
	21.0	40.00	34.80	0.00	–0.00	–0.77	8, 9, 10, 11, 12	II
	46.0	40.00	48.75	0.00	–0.00	–6.00	4, 6, 7, 13, 14	III

Note: Model A13 is equal to the length and width of each subfault. Model B13 is equal in width to each subfault, but the lengths are not equal. Each subfault is arranged from south to north.

Although the calculated value of model B13 can better fit the GPS data than other model's, the difference between the calculated value and GPS data is quite obvious at the point CHDU which is far from the fault, indicating that the fault plane is not fine enough along the width direction, and the fault needs to be refined in the width direction. We divided the entire fault plane into A23a, A23b, and A23c models based on the condition that the lengths of the subfaults are equal but the widths are unequal; According to the condition that the lengths of the sub-faults are not equal and the widths are not equal, the entire fault plane was divided into B23a, B23b, and B23c models (The distrib-

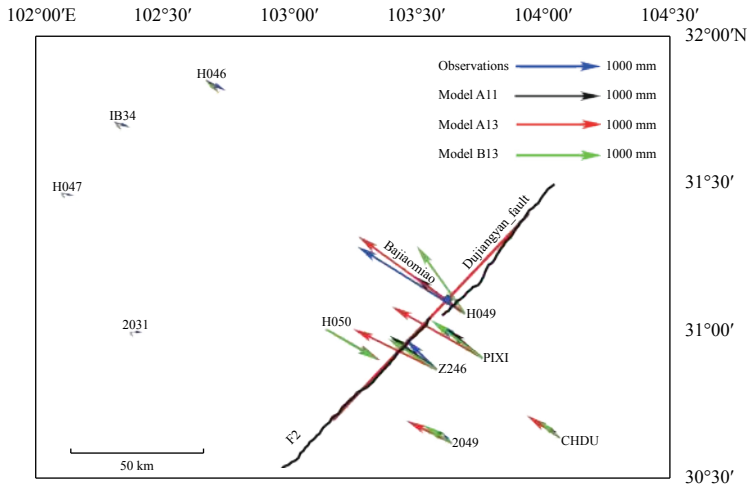


Figure 5 Comparison of surface displacement calculation by A11, A13, B13 and GPS observations. Blue is the ground-level GPS observations. The ground displacement of the A11 model is black, the A13 model is red, and the B13 model is green

ution of sub-faults in each model is shown in Figure 6. The geometric parameters and sliding parameters of each model are shown in Table 4, and the result of surface displacement calculated according to the model is shown in Figure 7.

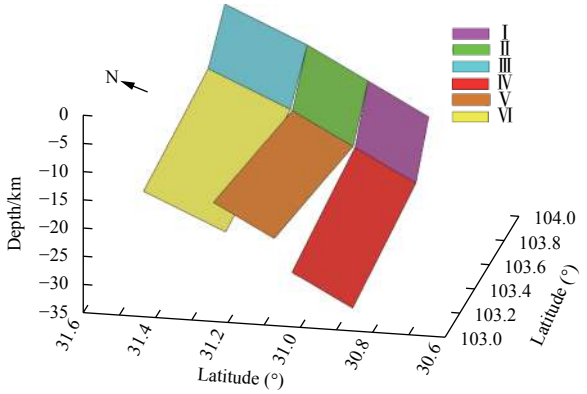


Figure 6 Sub-fault plane of 2 (row) × 3 (column) model schematic

When using the models A23a, A23b, and A23c, the displacement calculation values of the points H050, PIXI, and CHDU are all well fitted to the GPS observation values. In addition to the difference between the forward calculation value of the model A23a at the point H049 and the GPS observation is large, but the forward value of the model A23a at the point Z246 is better than the models A23b, A23c. Models B23a, B23b, and B23c are all superior to models A23a, A23b, and A23c, based on the calculation results of each model. The main differences between model B23a, B23b, and B23c are the calculated values of point Z246 and point CHDU. The calculated results of the B23a and B23b models at the near point Z246 are consistent with the GPS observations in the direction, but the calculated value of the model B23b is closer to the GPS observation than the model B23a in length. The calculated value of the displacement of the model B23c is not only longer in length but also more superior to the calculated value of the model B23b in the direction. At the point farther from the fault CHDU, the calculation result of the model B23c is also closer to the GPS observation than the results of the model B23a and B23b, which proves that the division of the model B23c in the width direction is more reasonable than the model B23a, B23b. According to the B23c model, the dip angle of the fault plane at the 11 km distance from the surface of the northern section of the Dujiangyan fault is 64.15°, close to 62° which is from the result of 590 m deep scientific drilling of the octagonal temple village (see Figure 7 blue square position). (Li et al., 2010), so we think that in the current fault division, B23c is the optimal fault model.

5 Discussion and conclusions

The dip angle of the fault in the Dujiangyan section of this paper is 45.1°, which is based on multiple focal mechanism solutions near the fault plane. To verify the accuracy of this result, based on the active tectonic map and seismicity, and based on the aftershocks catalog of magnitude 4.0 or higher (Wang et al., 2010), we determine the dip angle of the fault according to the maximum likelihood estimation method (Gao et al., 2016). In Figure 8, when the dip angle is equal to 44.1°, the objective function value is minimized and the fitting residual is minimized. At the same time, the fitting correlation reaches its maximum, and the dip difference from the focal mechanism solution is only 1.0°. This shows that the two results are consistent.

Table 4 Fault geometric model of 2 (row) ×3 (column)

Model	Length (km)	Width (km)	Dip/°	Depth (km)	Strike-slip U_1 (m)	Dip-slip U_2 (m)	Include focal point number	Subfault block number
A23a	33.3	20.0	53.18	0.0	–0.75	–4.45	1, 2	Ⅰ
	33.3	20.0	64.10	0.0	–0.00002	–3.70	9, 10, 12	Ⅱ
	33.3	20.0	51.97	0.0	–2.95	–9.99	4, 6, 13, 14	Ⅲ
	33.3	20.0	46.38	17.9	–0.014	–0.018	3, 5	Ⅳ
	33.3	20.0	27.28	17.9	–1.17	–0.0001	8, 11	Ⅴ
	33.3	20.0	32.91	17.9	–0.0004	–0.0002	7	Ⅵ
A23b	33.3	15.0	70.56	0.0	–3.54	–8.44	1	Ⅰ
	33.3	15.0	67.41	0.0	–0.00	–9.34	9, 10	Ⅱ
	33.3	15.0	64.15	0.0	–1.77	–9.99	13	Ⅲ
	33.3	25.0	45.55	13.8	–0.0007	–1.53	2, 3, 5	Ⅳ
	33.3	25.0	29.17	13.8	–0.0001	–0.001	8, 11, 12	Ⅴ
	33.3	25.0	44.25	13.8	–0.0006	–0.038	4, 6, 7, 14	Ⅵ
A23c	33.3	12.0	70.56	0.0	–3.96	–6.83	1	Ⅰ
	33.3	12.0	67.41	0.0	–0.00	–8.23	9, 10	Ⅱ
	33.3	12.0	64.15	0.0	–1.25	–9.99	13	Ⅲ
	33.3	28.0	45.55	11.1	–0.000	–2.77	2, 3, 5	Ⅳ
	33.3	28.0	29.17	11.1	–0.0003	–0.0002	8, 11, 12	Ⅴ
	33.3	28.0	44.25	11.1	–0.0006	–5.42	4, 6, 7, 14	Ⅵ
B23a	33.0	20.0	53.18	0.0	–0.00	–4.38	1, 2	Ⅰ
	21.0	20.0	64.10	0.0	–0.00	–1.63	9, 10, 12	Ⅱ
	46.0	20.0	51.97	0.0	–0.26	–8.59	4, 6, 13, 14	Ⅲ
	33.0	20.0	46.38	17.9	–0.0003	–4.44	3, 5	Ⅳ
	21.0	20.0	27.28	17.9	–4.29	–5.01	8, 11	Ⅴ
	46.0	20.0	32.91	17.9	–0.01	–0.02	7	Ⅵ
B23b	33.0	15.0	70.56	0.0	–0.003	–5.01	1	Ⅰ
	21.0	15.0	67.41	0.0	–0.00	–0.00	9, 10	Ⅱ
	46.0	15.0	64.15	0.0	–0.62	–9.99	13	Ⅲ
	33.0	25.0	45.55	13.8	–0.94	–8.26	2, 3, 5	Ⅳ
	21.0	25.0	29.18	13.8	–1.13	–0.006	8, 11, 12	Ⅴ
	46.0	25.0	44.25	13.8	–0.0001	–3.10	4, 6, 7, 14	Ⅵ
B23c	33.0	12.0	70.56	0.0	–0.01	–5.61	1	Ⅰ
	21.0	12.0	67.41	0.0	–0.00	–0.00	9, 10	Ⅱ
	46.0	12.0	64.15	0.0	–0.20	–9.08	13	Ⅲ
	33.0	28.0	45.55	11.1	–0.51	–5.53	2, 3, 5	Ⅳ
	21.0	28.0	29.18	11.1	–1.21	–0.00	8, 11, 12	Ⅴ
	46.0	28.0	44.25	11.1	–0.01	–2.42	4, 6, 7, 14	Ⅵ

Note: Model A23 is equal in length for each sub-fault, a, b, and c respectively represent different widths; model B23 is unequal in length for each sub-fault, and a, b, and c respectively represent different widths. The sub-faults are arranged from south to north and from shallow to deep.

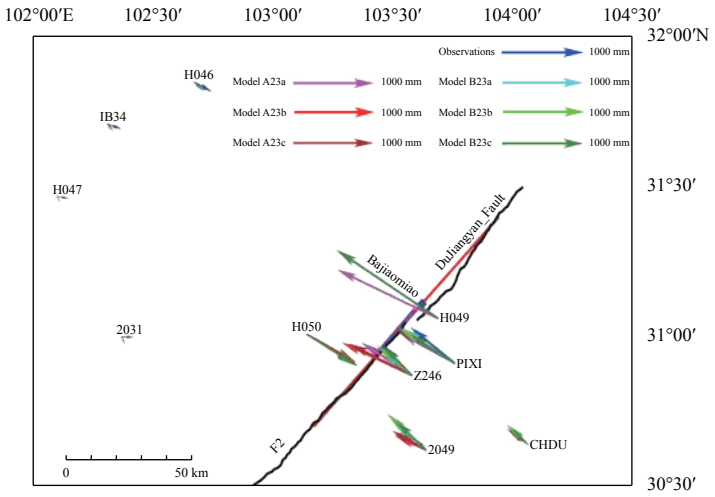


Figure 7 Comparison of surface displacement calculation by A23a, A23b, A23c,B23a, B23b, B23c and GPS observations

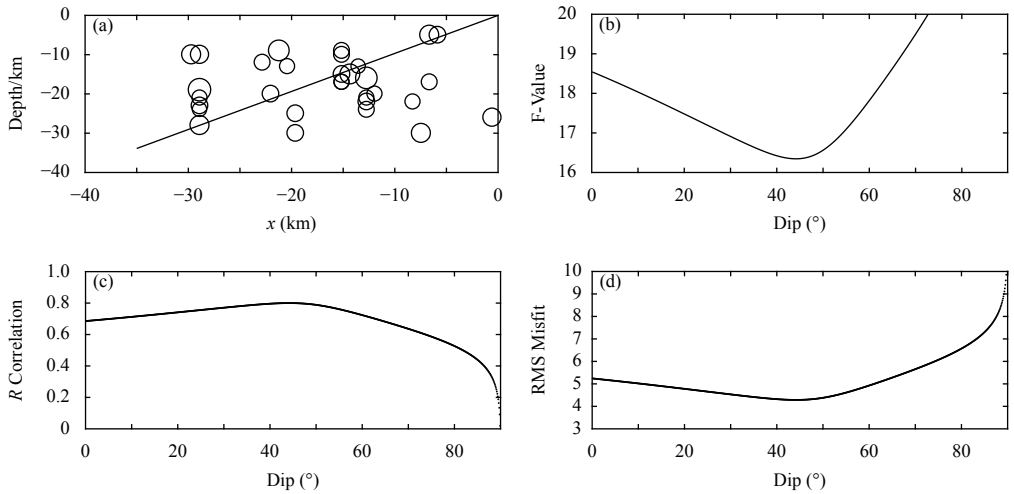


Figure 8 Dip angle of fault determine by GS method. In Figure 8a, establish a graph coordinate system with the midpoint of the fault ground line as the origin *O*, the *z* axis vertical to the ground as the depth direction, the *x* axis the vertical *z* axis as the horizontal distance direction, and the small circle as the earthquake source. Distribution, the black straight line is the result of the GS plane fitting, and the angle with the horizontal axis is the inclination of the fault plane at this reference point. (b) the result of the change of the objective function with the inclination angle, (c) the fitting correlation analysis, and (d) the result of the residual analysis of the objective function

In this paper, the division of sub-faults was divided into two types in the length direction: One type is divided into equal lengths, and the results are 33.3 km, 33.3 km, and 33.3 km respectively. The other type is divided according to the location of the faults on the surface of the main central fault (*F*2) in the Longmenshan. The results are 33 km, 21 km, and 46 km, respectively, with a median length of 21 km (see the purple line in Figure 7). The sub-fault planes was divided into a shallow 20 km and a deep 20 km in the width direction, 15 km in shallow portions and 25 km in deep portions. The second result is shallow 15 km and deep 25 km, The third result is shallow 12 km and deep 28 km. According to the length and width of various sub-faults, 9 geometric models are constructed, such as A11, A13, B13, A23a, A23b, A23c, B23a, B23b, and B23c.

The inversion results of each model show that the Longmenshan central fault zone is mainly characterized by reverse fault activity and a small amount of strike-slip. At the same time, it also shows that the existence of strike-slip components may make fault diversion easier at high dip angle.

From the point of view of the fit of the results of calculation points with the GPS observations on the

ground, the model A23b is better than the model A23a, the model A23c is better than the model A23b, the model B23b is better than B23a, and the model B23c is better than B23b. It suggested the reverse fault activity in the deep gently dipping angle to the shallow part. High-angled retrograde faults have a significant role in promoting earthquakes. The greater the width of the deep gentle angle fault plane, the smaller the width of the shallow high-angle fault plane, the more obvious this kind of acceleration effect. From Figure 7, we can see that except that the fitting result of the point 2049 is poor, the fitting results of the other points of the best model B23c are basically consistent with the GPS observation results. For the reasons that cause this result, we judge that point 2049 is located in the southern neighborhood of the fault and far from the fault, it is affected by sub-faults deep in the southern segment; The displacement of point 2049 is consistent with the direction of the GPS, indicating that the proportion of the components of strike-slip and dip-slip is correct. Although the length of displacement is slightly larger, It may be that $U_1 = -0.51$ m $U_2 = -5.53$ m are too large; It may also be that the sub-fault-slipping is not uniform and it is necessary to refine the fault to calculate more detailed results to make a more reasonable explanation.

In addition, field surveys after the earthquake indicate that at least the central fault and the piedmont faults have undergone dislocations during the process of major earthquakes (Xu et al., 2008; Zhang et al., 2009). However, this paper did not consider that the piedmont faults have been shifted. At the same time, we can see from Table 4 that the shallow that the dislocation amount of fault 21 km long shallow is 0 in the middle segment of the B23c model. This is consistent with the vacancy of the 20-km sliding distance from 80–100 km south of Beichuan (Wang et al., 2011).

This paper mainly studies the dip angle of the Dujiangyan section, based on the data of multiple focal mechanism solutions near the fault. The plane fault model with average dip angle and sub-fault model divided by length and width of the fault plane is studied. The optimal model B23c is obtained through inversion calculation and forward calculation with GPS data, based on dislocation theory.

That is, when the top of the fault is on the ground and has a width of 12 km, starting from the south end of the Dujiangyan fault, the lengths of subfaults are 33 km, 21 km, and 46 km, respectively, and the corresponding dip angle are 70.56°, 67.41°, and 45.55°, respectively. When the distance from the top of the fault to the surface is 11 km, the fault width is 28 km, and the lengths are 33 km, 21 km, and 46 km, respectively, and the corresponding dip angle are 44.55°, 29.18°, and 44.25°, respectively. The dip angle of the fault in Dujiangyan is consistent with the previous results of the deep gentle dip and shallow high dip angles of the Longmenshan fault.

The work carried out in this paper only involves 14 focal mechanism solutions for the thrust type from January 2008 to May 2009. Since there are no enough data points, the fault model cannot be refined. In order to obtain more accurate and precise fault geometry models, more reliable focal mechanism solutions, geophysical observations, and other data request be collected for further research.

Acknowledgments

This study was financially supported by the National Natural Science Foundation of China under Grant No.41304013 Science and Technology Project Plan of Weinan of 2016 No.2016KYJ-1-1 and State Key Laboratory of Geo-information Engineering No.SKLGIE2017-M-3-3. Parts of the figures were plotted with GMT software (Wessel and Smith, 1998). At the same time, express my sincere respect and heartfelt thanks to the reviewers for the valuable revisions proposed in this article.

References

Aki K (2008) Generation and propagation of G waves from the Niigata earthquake of June 16, 1964, 2, Estimation of the earthquake moment, released energy, and stress-strain drop from G wave spectrum. Bull.Earthquake Res. Inst. Tokyo **44**(18): 73–88

Burchfiel B, Royden L, Hilst V, Hager B, Chen Z, King R, Li C, Lü J, Yao H and Kirby E (2008) A geological and geophysical context for the Wenchuan earthquake of 12 May 2008, Sichuan, People's Republic of China. Gsa Today **18**(18): 4–11

Cui XF, Hu XP, Yu CQ, Tao K, Wang YH and Ning JY (2011) Research on focal mechanism solutions of Wenchuan earthquake sequence. Acta Scientiarum Naturalium Universitatis Pekinensis **47**(6): 1 063–1 072

Diao FQ, Xiong X, Wang RJ, Zheng Y and Hsu H (2010) Slip model of the 2008 M_W7.9 Wenchuan (China) earthquake derived from co-seismic GPS data. Earth Planets Space **62**(11): 869–874

Feng M, Zhang JZ and An MJ (2013) Tectonic stress changes around the epicenter before and after the 2008 Wenchuan earthquake. Seismol Geol **35**(4): 701–720

Frepoli A, Cimini GB, Gori PD, Luca GD, Marchetti A, Monna S, Montuori C and Pagliuca NM (2017) Seismic sequences and swarms in the Latium-Abruzzo-Molise Apennines (central Italy): New observations and analysis from a dense monitoring of the recent activity. Tectonophysics 712

Gao B, Zhou SY and Jiang CS (2016) Estimate of dip angles of faults around Ordos Block based on earthquakes. Chin J Geophys **59**(7): 2 444–2 452 (in Chinese with English abstract)

Guo XY, Chen XZ and Li YE (2010) Focal Mechanism Solutions for the 2008 M_S8.0 Wenchuan Earthquake and Part of its Aftershocks. Earthquake **30**(1): 50–60

Hayes G and Wald D (2010) Developing framework to constrain the geometry of the seismic rupture plane on subduction interfaces a priori- a probabilistic approach. Geophysical Journal of the Royal Astronomical Society **176**(3): 951–964

Hu XP, Yu CQ, Tao K, Cui XF, Ning JY and Wang YH (2008) Focal mechanism solutions of Wenchuan earthquake and its strong aftershocks obtained from initial P wave polarity analysis. Chinese J Geophys **51**(6): 1711–1718 ((in Chinese with English abstract)

Ji C and Hayes G (2009). Preliminary result of the May 12, 2008 M_W 7.9 eastern Sichuan, China earthquake. http://earthquake.usgs.gov/eqcenter/eqinthenews/2008/us2008ryan/finitefault.php, 2008.

Li F and Huang JS (2011) Numerical simulation of influences of medium heterogeneity and dip of fault on coseismic displacement. J Geode Geodyn **31**(5): 52–60

Li HB, Xu ZQ, Wang H, Si JL, Li TF, Song SR, Pei JL, Guo LW, Sun ZM, Huang Y, Chevalier ML and Liu DL (2013) The principle slip zone of the 2008 Wenchuan earthquake: A thrust fault oblique cutting the Yingxiu-Beichuan fault zone. Geology in China **40**(1): 121–139

Li HB, Si JL, Pei JL, Fu XF, Wang ZX, Li N, Hou Liwei, Wu FY and Pan JW (2010) Investigating the surface rupture process of the wenchuan earthquake (8.0). Quaternary Sciences **30**(4): 677–698

Li TM, Shen ZK, Xu J and Wan YG (2007) Analysis on the parameters of seismogenic fault of the earthquake more than 6.5 in North China. Progress in Geophysics **22**(1): 95–103

Mishra S (2006) Global Optimization By Particle Swarm Method: A Fortran Program. Mpra Paper

China Crustal Movement Observation Network project team (2008) Co-seismic displacement of Wenchuan M_S8.0 Earthquake measured by GPS. Sinence in China **38**(10): 1195–1206

Okada Y (1985) Surface deformation due to shear and tensile faults in a half-space. Bull Seismol Soc Amer **92**(2): 1018–1040

Okal E (1980) Quantitative Seismology: Theory and Methods. American Scientist (4): 449–450

Silver PG and Jordan TH (1982) Optimal estimation of scalar moment. Geophys J International **70**(3): 755–787

Sheng S (2015) Study on the Crustal stress field and the fault plane parameter of Circum-Ordos block region pressure. Institute of Geophysics, China Earthquake Administration Doctoral Dissertation

Shen ZK, Sun JB, Zhang PZ, Wan YG, Wang M, Bürgmann R, Zeng YH, Gan WJ, Liao H and Wang QL (2009) Slip maxima at fault junctions and rupturing of barriers during the 2008 Wenchuan earthquake. Nature Geoscience **2**(10): 718–724

Tong XP, Bridget SK and Sandwell D (2014) Is there a discrepancy between geological and geodetic slip rates along the San Andreas Fault System? J Geophys Res Solid Earth **119**(3): 2 518–2 538

Wang FC, Cao HR and Wan YG (2010) Application of linear errors-in-variables model for determination main earthquake's fault parameters of Wenchuan Earthquake. J Appl Statis Manag **29**(3): 381–390

Wang FC, Wan YG, Qian XS, Zhang LJ and Zhang MD (2013) A new method for determining fault planes parameters according to earthquake clustering. Chin J Geophys **56**(2): 522-530 (in Chinese with English abstract)

Wang Q, Qiao XJ, Lan QG, Freymueller J, Yang SM, Xu CJ, Yang YL, You XZ, Tan K and Chen G (2011) Rupture of deep faults in the 2008 Wenchuan earthquake and uplift of the Longmen Shan. Nature Geoscience **4**(9): 634–640

Wang WM, Zhao LF, Li J and Yao ZX (2008) Rupture process of the M_S8.0 Wenchuan earthquake of Sichuan, China. Chin J Geophys **51**(5): 1403–1410 (in Chinese with English abstract)

Xu ZQ, Li HB and Wu ZL (2008) Wenchuan earthquake and scientific drilling. Acta Geologica Sinica **82**(12): 1613–1622

Xu XW, Zhang PZ., Weng XZ, Qin ZL,Chen GH and Zhu AL (2005) Features of active tectonics and recurrence behaviors of strong earthquakes in the western Sichuan province and its adjacent regions. Seismol Geol **27**(3): 446–461

Xu XW, Wen XZ, Ye JQ, Ma BQ, Chen J, Zhou RJ, He HL, Tian QJ, He YL, Wang ZC, Sun ZM, Feng XJ, Yu GH, Chen LC, Chen GH, Yu S, Ran YK, Li XG, Li CX and An YF (2008) The M_S8.0 Wenchuan earthquake surface ruptures and its seismogenic structure. Seismol Geol **30**(3): 597–629

Xue TX, Fu RS and Lin F (2009a) The simulation of activities of bend fault. Chin J Geophys **52**(10): 2 509–2 518

Zhang LP, Shao ZG, Ma HS, Wang XZ and Li ZH (2013) The plate contact geometry investigation based on earthquake source parameters at the Burma arc subductionzone. Science China Earth Sciences **56**: 806–817

Zhang Y, Xu LS and Chen YT (2009) Spatio-temporal variation of the source mechanism of the 2008 great Wenchuan earthquake. Chin J Geophys **52**(2): 379–389

Zhang PZ (2008) Present-day tectonic deformation, strain distribution and deep dynamical processes in the western Sichuan basin in the eastern margin of the Tibetan Plateau. Science China **38**(9): 1041–1056

Zhang PZ, Wen XZ and Xu XW (2009) Tectonic model of the great Wenchuan earthquake of May 12, 2008, Sichuan, China. Chin Sci Bull **54**(7): 944–953 (in Chinese with English abstract)